

## TESTING THE DARK ENERGY WITH GRAVITATIONAL LENSING STATISTICS

SHUO CAO<sup>1,2</sup>, GIOVANNI COVONE<sup>2,3</sup>, AND ZONG-HONG ZHU<sup>1</sup>

<sup>1</sup> Department of Astronomy, Beijing Normal University, 100875 Beijing, China

<sup>2</sup> Dipartimento di Scienze Fisiche, Università di Napoli “Federico II,” Via Cinthia, I-80126 Napoli, Italy

<sup>3</sup> INFN Sez. di Napoli, Compl. Univ. Monte S. Angelo, Via Cinthia, I-80126 Napoli, Italy

Received 2012 February 21; accepted 2012 June 4; published 2012 July 24

### ABSTRACT

We study the redshift distribution of two samples of early-type gravitational lenses, extracted from a larger collection of 122 systems, to constrain the cosmological constant in the  $\Lambda$ CDM model and the parameters of a set of alternative dark energy models (XCDM, Dvali-Gabadadze-Porrati, and Ricci dark energy models), in a spatially flat universe. The likelihood is maximized for  $\Omega_\Lambda = 0.70 \pm 0.09$  when considering the sample excluding the Sloan Lens ACS systems (known to be biased toward large image-separation lenses) and no-evolution, and  $\Omega_\Lambda = 0.81 \pm 0.05$  when limiting to gravitational lenses with image separation  $\Delta\theta > 2''$  and no-evolution. In both cases, results accounting for galaxy evolution are consistent within  $1\sigma$ . The present test supports the accelerated expansion, by excluding the null hypothesis (i.e.,  $\Omega_\Lambda = 0$ ) at more than  $4\sigma$ , regardless of the chosen sample and assumptions on the galaxy evolution. A comparison between competitive world models is performed by means of the Bayesian information criterion. This shows that the simplest cosmological constant model—that has only one free parameter—is still preferred by the available data on the redshift distribution of gravitational lenses. We perform an analysis of the possible systematic effects, finding that the systematic errors due to sample incompleteness, galaxy evolution, and model uncertainties approximately equal the statistical errors, with present-day data. We find that the largest sources of systemic errors are the dynamical normalization and the high-velocity cutoff factor, followed by the faint-end slope of the velocity dispersion function.

*Key words:* cosmological parameters – gravitational lensing: strong – methods: statistical

*Online-only material:* color figures

### 1. INTRODUCTION

In the last 15 years, several complementary observational probes on cosmological scales have found strong evidence for an accelerating expansion of the universe: distance measurements of distant Type Ia supernovae (SNe Ia; Riess et al. 1998; Perlmutter et al. 1999), the observations of the cosmic microwave background anisotropies (*WMAP*; Bennett et al. 2003), and the baryon acoustic oscillations (BAOs) in the power spectrum of matter extracted from galaxy catalogs (Percival et al. 2007). By assuming general relativity, a negative pressure component has been invoked as the most feasible mechanism for the observed acceleration. The cosmological constant  $\Lambda$ , with a constant equation-of-state (EoS) parameter  $w = -1$ , is the simplest way to provide such a mechanism, although it suffers from unsolved problems such as the fine-tuning and cosmic coincidence problems. Dynamical dark energy models have also been proposed in the literature, such as the quintessence (Ratra & Peebles 1988; Caldwell et al. 1998), phantom (Caldwell 2002), quintom (Feng et al. 2005, 2006; Guo et al. 2005), Dvali-Gabadadze-Porrati (DGP; Dvali et al. 2000; Zhu & Alcaniz 2005; Zhu & Sereno 2008), and Ricci dark energy (RDE) models (Gao et al. 2009; Li et al. 2010).

The existence of a large number of theoretical models not conflicting with the basic observation of the accelerating expansion has triggered a variety of observational tests, based, for instance, on the angular size–redshift data of compact radio sources (Alcaniz 2002; Zhu & Fujimoto 2002), the age–redshift relation (Alcaniz et al. 2003), the lookback time to galaxy clusters (Pires et al. 2006), x-ray luminosities of galaxy clusters, and the Hubble parameter data (Gaztañaga et al. 2009; Stern et al. 2010; Cao et al. 2011a, 2011b). In

this context, strong gravitational lensing plays an important role, providing cosmological tests, such as gravitational lensing statistics (Kochanek 1996a; Zhu 1998; Cooray & Huterer 1999; Chiba & Yoshii 1999; Chae et al. 2002; Sereno 2005; Biesiada et al. 2010; Cao et al. 2011c, 2012; Cao & Zhu 2012), Einstein rings in galaxy-quasar systems (Yamamoto & Futamase 2001), clusters of galaxies acting as lenses on background high-redshift galaxies (Sereno 2002; Sereno & Longo 2004), and time delay measurements (Schechter 2005). Results from techniques based on gravitational lensing are complementary to other methods and can provide restrictive limits on the cosmological parameters. In this paper, we focus on one interesting lensing statistic suggested by Kochanek (1992) and further discussed and developed in literature (e.g., Helbig & Kayser 1996; Ofek et al. 2003).

Fukugita et al. (1990, but see also Nemiroff 1989) showed that the expected mean redshift of the lens increases with a larger cosmological constant  $\Omega_\Lambda$ . Kochanek (1992) obtained a formula for the probability distribution of the lens-galaxy redshift, as a function of the cosmological parameters given the source redshift and the image separation. Using a sample of four lenses, he found that a null cosmological constant is much more favorable than a flat cosmology with  $\Omega_\Lambda > 0.9$ . The redshift distribution test was reexamined by Helbig & Kayser (1996), who compared the redshifts of six lensing galaxies with the probabilities predicted by different cosmological models, assuming no galaxy evolution and that lensing galaxies could not be detected beyond a certain magnitude. In order to consider the selection effect introduced by the detectability of the lens galaxy, Kochanek (1996a) also took into account lensing systems with an absent lens redshift and obtained an upper limit of  $\Omega_\Lambda < 0.9$  at the 95% CL in a flat universe. Ofek et al. (2003)

rederived Kochanek’s expression for the expected lens redshift distribution, by allowing for number and mass evolution of the lens population, and applied this method to constrain both the cosmological and mass-evolution parameter spaces. They found that, for a flat universe and no lens evolution, only an upper limit could be obtained on the cosmological constant:  $\Omega_\Lambda < 0.89$  at the 95% CL.

Compared with other closely related tests based on the full lensing probability distribution, e.g., as a function of image separation, absolute numbers, etc., the differential probability of Kochanek (1992) for the galaxy to produce a lens of a given source redshift and image separation is determined by integrating the full lensing probability distribution over lens redshifts, which means that all of the uncertainties in the absolute value of the optical depth are eliminated. Moreover, this relative probability cuts off more sharply at high redshift than the total optical depth, since the constraints on the critical radius introduce an exponential term from the Schechter function beyond the redshift at which a  $\sigma_*$  galaxy is required to produce the observed separation. Indeed, this sharp cutoff makes the quantity  $d\tau/dz_l(\Delta\theta, z_s)$  a powerful cosmological tool.

Following works investigating the evolving lens population have concluded that galaxy evolution is not strongly constrained by the redshift distribution test and does not significantly affect lensing statistics (Mitchell et al. 2005; Capelo & Natarajan 2007; Oguri et al. 2012). However, the evolution of mass and number density can introduce large statistical errors and bias in the analysis of the lens redshift distribution. For example, a scarcity of lenses at higher redshifts may be due to evolution rather than to the smaller comoving volume due to a lower value of  $\Omega_\Lambda$ . Therefore, it is mandatory to consider the mass and density evolution into the statistical analysis of the redshift distribution of gravitational lenses. Other limitations include systematic effects due to a sample of gravitational lenses for which completeness might be not homogenous as a function of the lensed image separation and the lens redshift (Capelo & Natarajan 2007).

Oguri et al. (2012) have presented a comprehensive statistical analysis of the sample of 19 lensed quasars found in the Sloan Digital Sky Survey (SDSS) Quasar Lens Survey (SQLS). This sample is used to determine both the cosmological constant and evolution of the massive lensing galaxies. When considering a no-evolution case, a null cosmological constant is rejected at  $6\sigma$  level, providing independent evidence for the accelerated expansion.

The purpose of this paper is to extend our previous statistical analysis based on the angular separation distribution of the lensed images (Cao et al. 2011c) by using the redshift distribution test to obtain novel constraints on the parameters of spatially flat cosmological models. With this aim, we use a large sample of 122 gravitational lenses drawn from the Sloan Lens ACS (SLACS) Survey and other sky surveys.

The first aim is to obtain new constraints on the cosmological constant, by assessing both statistical and systematic uncertainties, mainly due to galaxy evolution and sample selection. Then, we also compare a number of alternative dark energy models with different numbers of parameters, in our analysis we apply, following Davis et al. (2007) and Li et al. (2010), a model comparison statistic, i.e., the so-called Bayesian information criterion (BIC; Schwarz 1978).

With respect to recent works (Oguri et al. 2012), we use a larger, not homogeneous sample and focus our attention on the determination of the cosmological constant and the comparison

with other alternative dark energy models, as the current sample size does not allow a firm determination of the rate of mass and number evolution of massive galaxies.

The paper is organized as follows. In Section 2, the basics of gravitational lensing statistics are introduced, also allowing for number and mass evolution of the lens population. We conduct a literature survey for known systems, listing their basic parameters and defining two statistical samples to perform the redshift test. In Section 3, we introduce four cosmological models, and show the results of constraining cosmological parameters using the Markov Chain Monte Carlo method, with and without galaxy evolution. In Section 4, we assess the possible presence of selection effects and systematic biases in our galaxy sample. Finally, we present the main conclusions and discussion in Section 5.

## 2. THE REDSHIFT TEST AND THE SAMPLE

The differential optical depth to lensing per unit redshift is

$$\frac{d\tau}{dz_l} = n(\Delta\theta, z_l)(1+z_l)^3 S_{\text{cr}} \frac{cdt}{dz_l}, \quad (1)$$

where  $n(\theta, z_l)$  is the comoving number density of lenses at redshift  $z_l$  producing an image separation  $\Delta\theta$ .  $S_{\text{cr}}$  is the cross-section for lensing, and  $cdt/dz_l$  is the proper distance interval.

Early-type galaxies are accurately described as singular isothermal spheres (SIS), and it is shown that radial mass distribution and ellipticity of the lens galaxy are unimportant in altering the cosmological constraints (Maoz & Rix 1993; Kochanek 1996b). The SIS density profile is

$$\rho(r) = \frac{\sigma^2}{2\pi G} \frac{1}{r^2}, \quad (2)$$

where  $\sigma$  is the velocity dispersion and  $r$  is the projected distance from the galaxy center. In Section 4, we will discuss the systematic uncertainties introduced by this assumption. The corresponding strong lensing cross-section is

$$S_{\text{cr}} = 16\pi^3 \left(\frac{\sigma}{c}\right)^4 \left(\frac{D_l D_{ls}}{D_s}\right)^2, \quad (3)$$

where  $D_l$ ,  $D_s$ , and  $D_{ls}$  are the angular diameter distances between the observer and the lens, the lens and the source, and the observer and the source, respectively (Ofek et al. 2003). Under a Friedman–Walker metric with null space curvature, the angular diameter distance reads

$$D_A(z_1, z_2; \mathbf{p}) = \frac{c}{H_0(1+z_2)} \int_{z_1}^{z_2} \frac{dz'}{E(z'; \mathbf{p})}, \quad (4)$$

where  $H_0$  is the Hubble constant and  $E(z; \mathbf{p})$  is the dimensionless expansion rate dependent on redshift  $z$  and cosmological model parameters  $\mathbf{p}$ . The two multiple images will form at an angular separation

$$\Delta\theta = 8\pi \left(\frac{\sigma}{c}\right)^2 \frac{D_{ls}}{D_s}. \quad (5)$$

In order to derive the differential optical depth, we use the empirically determined velocity dispersion distribution function (VDF) of early-type galaxies: following previous works, we limit our sample to lensing early-type galaxies. The VDF is

generally modeled by a modified Schechter function of the form (Sheth et al. 2003)

$$\frac{dn}{d\sigma} = n_* \left( \frac{\sigma}{\sigma_*} \right)^\alpha \exp \left[ - \left( \frac{\sigma}{\sigma_*} \right)^\beta \right] \frac{\beta}{\Gamma(\alpha/\beta)} \frac{1}{\sigma}, \quad (6)$$

where  $\alpha$  is the faint-end slope,  $\beta$  the high-velocity cutoff, and  $n_*$  and  $\sigma_*$  are the characteristic number density and velocity dispersion, respectively. In the following analysis, we use the results of Choi et al. (2007), who analyzed data from the SDSS Data Release 5 to derive the VDF of early-type galaxies. They found  $n_* = 8.0 \times 10^{-3} h^3 \text{ Mpc}^{-3}$ , where  $h$  is  $H_0$  in units of  $100 \text{ km s}^{-1} \text{ Mpc}^{-1}$ ,  $\sigma_* = 161 \text{ km s}^{-1}$ ,  $\alpha = 2.32 \pm 0.10$ , and  $\beta = 2.67 \pm 0.07$ .

We also allow for evolution of the quantities  $n_*$  and  $\sigma_*$ , by adopting the following parameterization:

$$n_*(z_l) = n_*(1+z_l)^P, \quad \sigma_*(z_l) = \sigma_*(1+z_l)^U, \quad (7)$$

where  $P$  and  $U$  are constant quantities.

In the following, we check the effect of redshift evolution by letting  $P$  and  $U$  be free parameters in Section 3, instead of adopting the evolution of  $(P, U) = (-0.23, -0.01)$  predicted by the semi-analytic model of Kang et al. (2005) and Chae (2007). Moreover, since the main goal of this paper is to constrain cosmological parameters, we first consider  $P$  and  $U$  as free parameters, obtain their best-fit values and probability distribution function, and marginalize them to determine constraints on the relevant cosmological parameters of interest.

Straightforward calculations lead to the optical depth per unit redshift for a system with image separation  $\Delta\theta$  and source redshift  $z_s$ ,

$$\begin{aligned} \frac{d\tau}{dz_l}(\Delta\theta, z_s) &= \tau_N (1+z_l)^{[-U\alpha+P]} \\ &\times (1+z_l)^3 \frac{D_{ls}}{D_s} D_l^2 \frac{cdt}{dz_l} \left( \frac{\Delta\theta}{\Delta\theta_*} \right)^{\frac{1}{2}\alpha+1} \\ &\times \exp \left[ - \left( \frac{\Delta\theta}{\Delta\theta_*} \right)^{\frac{1}{2}\beta} (1+z_l)^{-U\beta} \right], \quad (8) \end{aligned}$$

where the normalization

$$\tau_N = 2\pi^2 n_* \frac{\beta}{\Gamma(\alpha/\beta)} \left( \frac{\sigma_*}{c} \right)^2, \quad (9)$$

and

$$\Delta\theta_* = 8\pi \left( \frac{\sigma_*}{c} \right)^2 \frac{D_{ls}}{D_s}. \quad (10)$$

For a given lens system, the dependence of  $d\tau/dz_l$  on  $z_l$  gives the relative probability of finding the lens at different redshift:

$$\begin{aligned} \delta p_l &= \frac{d\tau}{dz_l} / \tau \\ &= \frac{d\tau}{dz_l} / \int_0^{z_s} \frac{d\tau}{dz_l} dz_l. \quad (11) \end{aligned}$$

The total optical depth for multiple imaging of a compact source  $\tau$ , the probability that an SIS forms multiple images of a background source with angular separation  $\Delta\theta$ ,  $d\tau/d\Delta\theta$  (Cao et al. 2011c; Cao & Zhu 2012), and the probability of lensing by a deflector at  $z_l$ ,  $d\tau/dz_l$ , are obtained by integrating the differential probability in Equation (8).

Moreover, it should be noted that the method applied in this paper is not affected by the bias that larger separation lenses are more easily discovered, since the image separation is included only as a prior. This advantage allows us to use almost all the known lenses, regardless of their method of discovery (Kochanek 1992). We have compiled a list of 122 gravitational lenses from a variety of sources in literature. Their basic data (lens and source redshifts both and the largest image separations) are summarized in Table 1. As mentioned above, in order to build an homogeneous galaxy sample, we limit our analysis to galaxies with early-type morphology.

The main source is given by the SLACS project (Bolton et al. 2008), providing 59 lenses in our list. These lenses have redshifts in the range from  $z_l \simeq 0.05$  to 0.5, making the lower redshift part of our overall sample, with the lensed sources ranging from  $z_s \simeq 0.2$  to 1.2 (Bolton et al. 2008). As a consequence of the initial spectroscopic selection method, all the SLACS gravitational lenses have known spectroscopic redshifts for both source and lens, giving the SLACS sample an immediate scientific advantage over strong-lens candidate samples selected from imaging data. However, it is known that the SLACS sample is biased toward moderately large-separation lenses ( $\Delta\theta > 2''$ ; Arneson et al. 2012), leading to biased estimates in the redshift test (Capelo & Natarajan 2007).

A majority of the sample was observed as part of the CASTLES program,<sup>4</sup> but it also contains gravitational lenses found in the COSMOS survey<sup>5</sup> (Faure et al. 2008) and the Extended Growth Strip (EGS; Moustakas et al. 2007), including six additional COSMOS and EGS systems discovered recently: COSMOS5921+0638, COSMOS0056+1226, COSMOS0245+1430, ‘‘Cross,’’ and ‘‘Dewdrop.’’ Finally, we also include five early-type gravitational lenses from Lenses Structure and Dynamics survey (LSD; Koopmans & Treu 2002, 2003; Treu & Koopmans 2004), spanning the redshift range  $0.48 < z_l < 1.00$  (Q0047-2808, HST15433+5352, MG2016, CY2201-3201, and CFRS03.1077).

Moreover, lenses dominated by a group or cluster potential will affect the constraint results (Keeton & Zabludoff 2004; Oguri et al. 2005; Faure et al. 2011) and previous versions of the lens redshift test have certainly gone to some effort to exclude these systems. Therefore, systems known to be strongly affected by the presence of a group (e.g., B1359+154) or galaxy cluster (e.g., Q0957+561, SDSS1004+4112, and B2108+213) have been excluded from our sample. Moreover, we follow previous works in adopting the image-separation criterion of  $4''$  in order to remove lenses that are influenced by complex environments such as clusters (Ofek et al. 2003). On this basis, we have removed Q0047-2828 and RXJ0921+4529 from the final sample. However, it should be noted that the separation is used as prior information in calculating the lens redshift probability, even if we reject a lens that has a large separation, this criterion will not bias the technique because its lens redshift is very low relative to the source redshift (Ofek et al. 2003).

The redshift distribution test requires a statistically complete and well-characterized sample. As our list includes galaxies from a variety of surveys, using very different observational strategies and discovery spaces (the SDSS spectroscopic sample, *Hubble Space Telescope* (HST) field sky survey, etc.), it is mandatory to verify the completeness of our final sample of

<sup>4</sup> <http://cfa-www.harvard.edu/castles/>

<sup>5</sup> <http://cosmos.astro.caltech.edu/>

**Table 1**  
Summary of the Properties of the Strongly Lensed Systems, with the SLACS Lenses Written in Bold

Lens Name	$z_s$	$z_l$	$\Delta\theta(^{\circ})$	Ref	Lens Name	$z_s$	$z_l$	$\Delta\theta(^{\circ})$	Ref
<b>J0029-0055</b>	0.9313	0.227	1.92	1	J221929-001743	1.0232	0.2888	1.472	4
<b>J0037-0942</b>	0.6322	0.1955	2.943	1, 2	J022511-045433	1.1988	0.2380	3.54	4
<b>J0044+0113</b>	0.1965	0.1196	1.58	1, 3	J022610-042011	1.232	0.4943	2.306	4
<b>J0109+1500</b>	0.5248	0.2939	1.38	1	MG2016	3.263	1.004	3.12	5
<b>J0216-0813</b>	0.5235	0.3317	2.303	1, 2, 3	HST15433+5352	2.092	0.497	1.18	5, 6, 7
<b>J0252+0039</b>	0.9818	0.2803	2.08	1	CY2201-3201	3.900	0.320	0.830	5, 6, 7
<b>J0330-0020</b>	1.0709	0.3507	2.2	1, 3	CFRS03.1077	2.941	0.938	2.48	5, 6, 7
<b>J0405-0455</b>	0.8098	0.0753	1.6	1	Q0142-100	2.72	0.49	2.231	8
<b>J0728+3835</b>	0.6877	0.2058	2.5	1	PMNJ0134-0931	2.216	0.76451	0.7	9, 10, 11
<b>J0737+3216</b>	0.5812	0.3223	2.065	2, 3	B0218+357	0.944	0.685	0.33	12, 13, 14
<b>J0822+2652</b>	0.5941	0.2414	2.34	1	CFRS03.1077	2.941	0.938	2.1	15
<b>J0841+3824</b>	0.6567	0.1159	2.82	1	MG0414+0534	2.64	0.9584	2.12	16, 17
<b>J0912+0029</b>	0.3239	0.1642	3.23	1, 2	HE0435-1223	1.689	0.4	2.6	18
<b>J0935-0003</b>	0.467	0.3475	1.74	1, 3	HE0512-3329	1.565	0.9313	0.644	19
<b>J0936+0913</b>	0.588	0.1897	2.18	1	B0712+472	1.339	0.406	1.28	20
<b>J0946+1006</b>	0.6085	0.2219	2.76	1	MG0751+2716	3.200	0.3502	0.7	17
<b>J0955+0101</b>	0.3159	0.1109	1.82	1	HS0818+1227	3.115	0.39	2.55	21
<b>J0956+5100</b>	0.4699	0.2405	2.642	1, 2	SBS0909+523	1.377	0.830	1.10	22
<b>J0959+4416</b>	0.5315	0.2369	1.92	1, 2	RXJ0911+0551	2.80	0.77	3.25	23
<b>J0959+0410</b>	0.535	0.126	1.995	1	FBQ0951+2635	1.24	0.25	1.10	25
<b>J1016+3859</b>	0.4394	0.1679	2.18	1	BRI0952-0115	4.50	0.41	0.99	26
<b>J1020+1122</b>	0.553	0.2822	2.4	1	J100424.9+122922	2.65	0.95	1.54	27
<b>J1023+4230</b>	0.696	0.1912	2.82	1	LBQS1009-0252	2.74	0.88	1.53	28
<b>J1029+0420</b>	0.6154	0.1045	2.02	1	Q1017-207	2.545	1.085	0.849	29
<b>J1032+5322</b>	0.329	0.1334	2.06	1	FSC10214+4724	2.286	0.914	1.59	30
<b>J1103+5322</b>	0.7353	0.1582	2.04	1, 3	B1030+071	1.535	0.599	1.56	20
<b>J1106+5228</b>	0.4069	0.0955	2.46	1, 3	HE1104-1805	2.32	0.729	3.19	31
<b>J1112+0826</b>	0.6295	0.273	2.98	1, 3	PG1115+080	1.72	0.311	2.42	32
<b>J1134+6027</b>	0.4742	0.1528	2.2	1	B1152+200	1.019	0.439	1.56	33
<b>J1142+1001</b>	0.5039	0.2218	1.96	1, 3	Q1208+101	3.80	1.1349	0.47	34
<b>J1143-0144</b>	0.4019	0.106	3.36	1	HST14113+5211	2.811	0.465	2.26	22
<b>J1153+4612</b>	0.8751	0.1797	2.1	1	HST14176+5226	3.40	0.81	3.25	35
<b>J1204+0358</b>	0.6307	0.1644	2.62	1, 3	B1422+231	3.62	0.339	1.28	32
<b>J1205+4910</b>	0.4808	0.215	2.44	1	SBS1520+530	1.855	0.717	1.568	8, 36
<b>J1213+6708</b>	0.6402	0.1229	2.84	1, 3	MG1549+3047	1.17	0.11	2.3	37
<b>J1218+0830</b>	0.7172	0.135	2.9	1, 3	B1600+434	1.589	0.4144	1.38	20
<b>J1250+0523</b>	0.7953	0.2318	2.26	1, 2	B1608+656	1.394	0.630	2.27	38
<b>J1330-0148</b>	0.7115	0.0808	1.706	1, 2	PMNJ1632-0033	3.424	1.0	1.47	39
<b>J1402+6321</b>	0.4814	0.2046	2.775	1, 2	FBQ1633+3134	1.52	0.684	0.66	40
<b>J1403+0006</b>	0.473	0.1888	1.66	1	MG1654+1346	1.74	0.254	2.1	41
<b>J1416+5136</b>	0.8111	0.2987	2.74	1, 3	PKS1830-211	2.51	0.886	0.99	42
<b>J1420+6019</b>	0.5351	0.0629	2.097	1, 2	PMNJ1838-3427	2.78	0.31	1.00	43
<b>J1430+4105</b>	0.5753	0.285	3.04	1	B1933+507	2.63	0.755	1.00	44
<b>J1432+6317</b>	0.6643	0.123	2.52	1, 3	B2045+265	1.28	0.8673	2.2	45
<b>J1436-0000</b>	0.8049	0.2852	2.24	1, 3	HE2149-2745	2.03	0.50	1.69	8, 46
<b>J1443+0304</b>	0.4187	0.1338	1.62	1, 3	Q2237+0305	1.695	0.0394	1.82	47
<b>J1451-0239</b>	0.5203	0.1254	2.08	1, 3	SDSS0246-0825	1.68	0.724	1.2	48
<b>J1525+3327</b>	0.7173	0.3583	2.62	1, 3	B0850+054	3.93	0.59	0.68	49
<b>J1531-0105</b>	0.7439	0.1596	3.42	1, 3	SDSS0903+5028	3.605	0.388	3.0	50
<b>J1538+5817</b>	0.5312	0.1428	2	1, 3	HE1113-0641	1.235	0.75	0.88	51
<b>J1621+3931</b>	0.6021	0.2449	2.58	1, 3	Q1131-1231	0.658	0.295	3.8	52
<b>J1627-0053</b>	0.5241	0.2076	2.42	1, 2	SDSS1138+0314	2.44	0.45	1.34	53, 54
<b>J1630+4520</b>	0.7933	0.2479	3.618	1, 2	SDSS1155+6346	2.89	0.176	1.96	55
<b>J1636+4707</b>	0.6745	0.2282	2.18	1	SDSS1226-0006	1.12	0.52	1.26	53, 54
<b>J2238-0754</b>	0.7126	0.1371	2.54	1, 3	WFI2033-4723	1.66	0.66	2.34	53, 55
<b>J2300+0022</b>	0.4635	0.2285	2.494	1, 2	HE0047-1756	1.66	0.41	1.54	56
<b>J2303+1422</b>	0.517	0.1553	3.278	1, 2	COSMOS5921+0638	3.15	0.551	1.6	57, 58
<b>J2321-0939</b>	0.5324	0.0819	3.2	1, 2	COSMOS0056+1226	0.81	0.361	2.4	57, 59
<b>J2341+0000</b>	0.807	0.186	2.88	1, 3	COSMOS0245+1430	0.779	0.417	3.08	57, 59
J021737-051329	1.847	0.6458	2.536	4	“Cross”	3.40	0.810	2.44	60
J141137+565119	1.420	0.3218	1.848	4	“Dewdrop”	0.982	0.580	1.52	60

**References.** (1) Bolton et al. 2008; (2) Treu et al. 2006; (3) Newton et al. 2011; (4) Ruff et al. 2011; (5) Koopmans & Treu 2002; (6) Koopmans & Treu 2003; (7) Treu & Koopmans 2004; (8) Kochanek et al. 2000; (9) Winn et al. 2002a; (10) Gregg et al. 2002; (11) Hall et al. 2002; (12) O’Dea et al. 1992; (13) Wiklind & Combes 1995; (14) Cohen et al. 2003; (15) Crampton et al. 2002; (16) Falco et al. 1997; (17) Tonry & Kochanek 1999; (18) Wisotzki et al. 2002; (19) Gregg et al. 2000; (20) Fassnacht & Cohen 1998; (21) Hagen & Reimers 2000; (22) Lubin et al. 2000; (23) Kneib et al. 2000; (24) Muñoz et al. 2001; (25) Schechter et al. 1998; (26) Lehár et al. 2000; (27) Lacy et al. 2002; (28) Hewett et al. 1994; (29) Surdej et al. 1997; (30) Eisenhardt et al. 1996; (31) Lidman et al. 2000; (32) Tonry 1998; (33) Myers et al. 1999; (34) Siemiginowska et al. 1998; (35) Ratnatunga et al. 1999; (36) Burud et al. 2002b; (37) Lehár et al. 1993; (38) Fassnacht et al. 1996; (39) Winn et al. 2002b; (40) Morgan et al. 2001; (41) Langston et al. 1989; (42) Wiklind & Combes 1996; (43) Winn et al. 2000; (44) Sykes et al. 1998; (45) Fassnacht et al. 1999; (46) Burud et al. 2002a; (47) Huchra et al. 1985; (48) Inada et al. 2005; (49) Biggs et al. 2003; (50) Johnston et al. 2003; (51) Blackburne et al. 2008; (52) Sluse et al. 2003; (53) Eigenbrod et al. 2006; (54) Inada et al. 2008; (55) Morgan et al. 2004; (56) Ofek et al. 2006; (57) Faure et al. 2008; (58) Anguita et al. 2009; (59) Lagattuta et al. 2010; (60) Moustakas et al. 2007.

**Table 2**  
Summary of the Subsamples Used in the Analysis of This Paper

Subsample	Definition
Sample A	63 lenses from Table 1 excluding the SLACS sample
Sample B	71 lenses with image separation larger than 2''
Sample C	51 lenses with image separation not larger than 2''
SLACS	59 lenses from the whole SLACS sample
Full sample	122 lenses from Table 1

gravitational lenses and its usability for the redshift test. In our analysis, we will use the two following samples (see Table 2).

*Sample A.* Sixty-three lenses from the above list, excluding the whole SLACS sample. This sample is extracted by the same parent population as the primary sample investigated in Capelo & Natarajan (2007).

*Sample B.* Seventy-one lenses with image separation larger than 2''. This choice is motivated by the fact that the SLACS sample is biased toward moderately large-separation lenses and large velocity dispersions and is less than 50% complete below  $\Delta\theta = 2''$  (Arneson et al. 2012).

We will discuss the samples selection functions and the impact on our results in Section 4.

### 3. STATISTICAL ANALYSIS

Our statistical analysis is based on the maximum likelihood technique. For a sample of  $N_L$  multiply imaged sources, the likelihood  $\mathcal{L}$  of the observed lens redshift given the statistical lensing model is defined by

$$\ln \mathcal{L} = \sum_{l=1}^{N_L} \ln \delta p_l(\mathbf{p}), \quad (12)$$

where  $\delta p_l(\mathbf{p})$  is the particular differential probability given by Equation (11) normalized to one, and  $\mathbf{p}$  are the cosmological model parameters (e.g.,  $\Omega_\Lambda$ ,  $\Omega_m$ ), for the  $l$ th multiply imaged source. Accordingly, the  $\chi^2$  is defined as follows:

$$\chi^2 = -2 \ln \mathcal{L}. \quad (13)$$

The best-fit model parameters are determined by minimizing the total  $\chi^2$ . The 68.3% confidence level is determined by  $\Delta\chi^2 \equiv \chi^2 - \chi_{\min}^2 \leq 1.0$  and 2.3 for  $k = 1$  and 2, respectively, where  $k$  is the number of free model parameters. On the other hand, the 95.4% confidence level is determined by  $\Delta\chi^2 \equiv \chi^2 - \chi_{\min}^2 \leq 4.0$  and 6.17 for  $k = 1$  and 2, respectively. Our analysis is based on the publicly available package COSMOMC (Lewis & Bridle 2002).

We consider four different cosmological models to be tested with the observed lens redshift distribution: the  $\Lambda$ CDM model and three phenomenological models in which the vacuum energy is described as a dynamical quantity: the so-called XCDM model with the EoS  $w = p/\rho$  a free parameter, the DGP model arising from the brane world theory, and the RDE models. These models are motivated by the well-known fine-tuning and coincidence problems of the standard  $\Lambda$ CDM model.

We note that the previous precision cosmological observational data have hinted that both the RDE and dark energy with EoS  $w < -1$  may have dubious stability problems (Feng & Li 2009; Amani 2011), and the DGP model has already been ruled out observationally (Fang et al. 2008; Durrer & Maartens 2010; Maartens & Koyama 2010), so it is indicated that these are just

supposed to be a representative set, instead of viable candidates for dark energy.

It is well known that the  $\chi^2$ -statistics alone are not sufficient to provide an effective way to make a comparison between different models. Since, in general, a model with more parameters tends to give a lower  $\chi_{\min}^2$ , it is unwise to compare different models by simply considering  $\chi_{\min}^2$  with likelihood contours or best-fit parameters. Instead, the information criteria can be used to assess different models. In this paper, we use the BIC, also known as the Schwarz information criterion, as a model selection criterion (Schwarz 1978). The BIC is defined by

$$\text{BIC} = -2 \ln \mathcal{L}_{\max} + k \ln N, \quad (14)$$

where  $\mathcal{L}_{\max}$  is the maximum likelihood, and  $N$  is the number of the used data points. Note that for Gaussian distributions,  $\chi_{\min}^2 = -2 \ln \mathcal{L}_{\max}$ , and the difference in the BIC can be simplified to  $\Delta\text{BIC} = \Delta\chi_{\min}^2 + \Delta k \ln N$ . A difference in BIC ( $\Delta\text{BIC}$ ) of 2 is considered positive evidence against the model with the higher BIC, while a  $\Delta\text{BIC}$  of 6 is considered strong evidence.

A spatially flat universe is assumed throughout the paper, which is strongly supported by independent experiments: a combined 5-year *Wilkinson Microwave Anisotropy Probe* (WMAP5), BAOs, and SN data give  $\Omega_{\text{tot}} = 1.0050_{-0.0061}^{+0.0060}$  (Hinshaw et al. 2009). As mentioned above, we also consider the case of an evolving population of lensing galaxies in order to assess the accuracy of our results. We consider simultaneous constraints on the galaxy evolution and cosmological parameters. In order to derive the probability distribution function for the cosmological parameters of interest, we marginalize  $P$  and  $U$  and perform fits of different cosmological scenarios on both Samples A and B. Results are shown in Figures 1–6 and summarized in Table 5.

#### 3.1. The Standard Cosmological Model ( $\Lambda$ CDM)

In the simplest scenario, the dark energy is a cosmological constant,  $\Lambda$ , i.e., a component with constant EoS  $w = p/\rho = -1$ . If spatial flatness of the Friedman–Robertson–Walker metric is assumed, then the Hubble parameter according to the Friedmann equation is

$$H^2 = H_0^2 [\Omega_m (1+z)^3 + \Omega_\Lambda], \quad (15)$$

where  $\Omega_m$  and  $\Omega_\Lambda$  represent the density parameters of matter (both baryonic and non-baryonic components) and cosmological constant, respectively. As  $\Omega = \Omega_m + \Omega_\Lambda = 1$ , this model has only one independent parameter.

We consider constraints obtained for both samples defined above. While considering Sample A, the likelihood is maximized,  $\mathcal{L} = \mathcal{L}_{\max}$ , for  $\Omega_\Lambda = 0.70 \pm 0.09$  with no redshift evolution and  $\Omega_\Lambda = 0.73 \pm 0.09$  with redshift evolution, see Figure 1. Hereafter, uncertainties denote the statistical 68.3% confidence limit for one parameter, determined by  $\mathcal{L}/\mathcal{L}_{\max} = \exp(-1/2)$ . Data are consistent with the no-redshift-evolution case ( $P = 0$ ,  $U = 0$ ) at  $1\sigma$ . Specifically, the measured values of the two parameters are  $P = -1.2 \pm 1.4$  and  $U = 0.22_{-0.27}^{+0.26}$ .

When using the Sample B, we find, in the no-evolution scenario,  $\Omega_\Lambda = 0.81 \pm 0.05$ , consistent with the result from Sample A. When allowing for galaxy evolution, we find  $\Omega_\Lambda = 0.83 \pm 0.05$ ,  $P = -1.9 \pm 4.6$ , and  $U = 0.16 \pm 0.30$ .

In both cases, our findings are very close to the ones obtained from the ESSENCE supernova survey data,  $\Omega_\Lambda = 0.73 \pm 0.04$  in the flat case (Davis et al. 2007), and from the combined *WMAP*

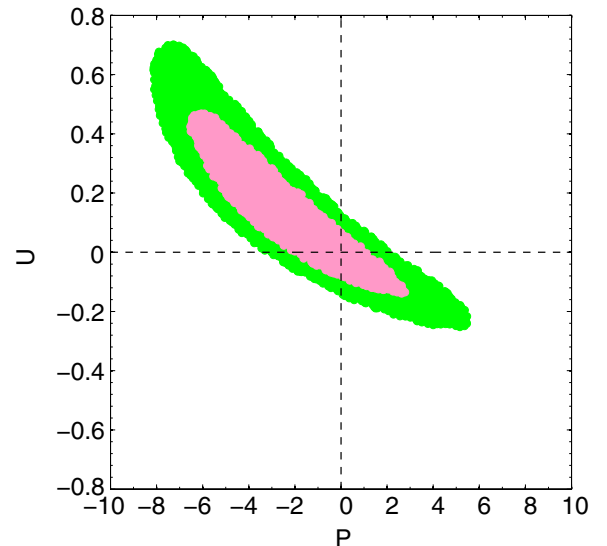
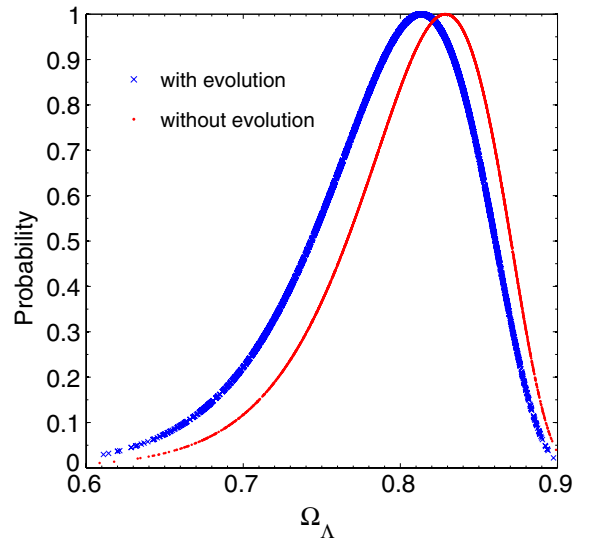
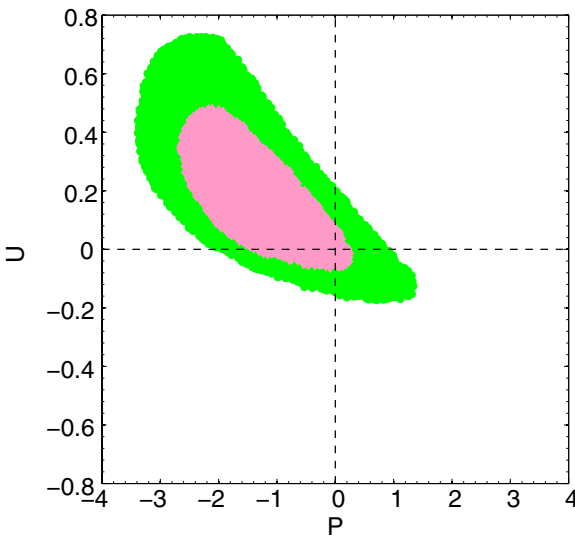
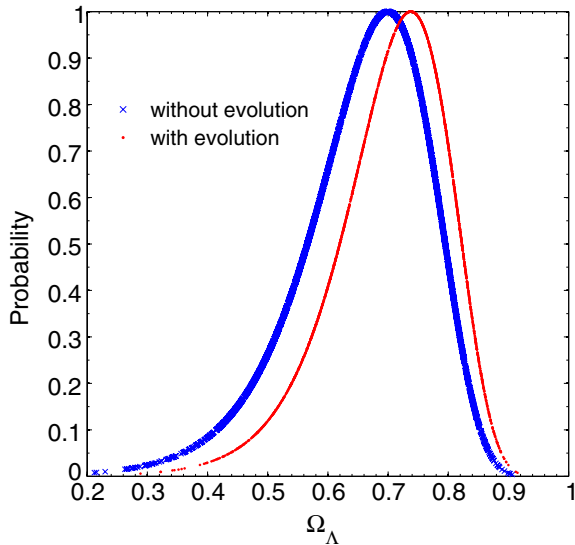


**Figure 1.** Simultaneous constraints on the cosmological constant and redshift evolution of the VDF of galaxies in the flat  $\Lambda$ CDM model obtained by using Sample A. Upper panel: likelihood distributions as a function of  $\Omega_\Lambda$  with and without redshift evolution. The red dotted line is the likelihood after marginalizing over the evolution parameters  $P$  and  $U$ . Lower panel: constraints on redshift evolution in the  $P-U$  plane after marginalizing over  $\Omega_\Lambda$ . Dashed lines in the lower panel indicate no redshift evolution ( $P = 0$  and  $U = 0$ ).

(A color version of this figure is available in the online journal.)

5-year, BAO, and SN Union data (Komatsu et al. 2009) with the best-fit parameter  $\Omega_\Lambda = 0.726 \pm 0.015$ . Moreover, both samples used here exclude with large confidence ( $4\sigma$  level) the null hypothesis of a vanishing  $\Omega_\Lambda$ , as obtained also by Oguri et al. (2012) in their statistical analysis on the SQLS data, providing independent evidence of the accelerated expansion.

While detailed analysis on the constraints of the redshift distribution test on the hierarchical models of galaxy evolution is beyond the scope of this work, we notice that these results obtained with both samples are in broad agreement with previous studies (Capelo & Natarajan 2007; Oguri et al. 2012), in which no strong evidence for any evolution of the parameters  $U$  and  $P$  was found. Our results support high-redshift formation and passive evolution of the population of massive early-type galaxies. Also note that the most degenerate direction in the evolution parameters roughly corresponds to a constant lensing optical depth, as already found by Oguri et al. (2012).

**Figure 2.** As in Figure 1, using Sample B (i.e., lensing systems with image separation larger than  $2''$ ).

(A color version of this figure is available in the online journal.)

Previous studies on lensing statistics (Chae 2003; Ofek et al. 2003) considering a not-evolving velocity dispersion function obtained results in agreement with the galaxy number counts (Im et al. 2002). Mitchell et al. (2005) have also investigated the effect of evolution of the velocity function on the lensing statistics, and they concluded that the simple evolution does not significantly affect lensing statistics if all galaxies are early type. More recently, Capelo & Natarajan (2007) assumed a non-evolving shape for the VDF and obtained results consistent with earlier results. To sum up, all previous results on redshift evolution from strong lensing statistics were based on the assumption of the non-evolving shape for the VDF and appeared to be consistent with no-evolution of early-type galaxies. As we only considered early-type lensing galaxies, our results further confirm this conclusion.

While our results are consistent with no-evolution, the constraints in the  $P-U$  plane are relatively weak. Studies of galaxy evolution have identified significant number and mass evolution in the early-type population from  $z = 0$  to 1 with a decline in the abundance by roughly a factor of two by  $z = 1$ , which corresponds to  $P \simeq -1$  (Faber et al. 2007; Brown et al. 2007) and

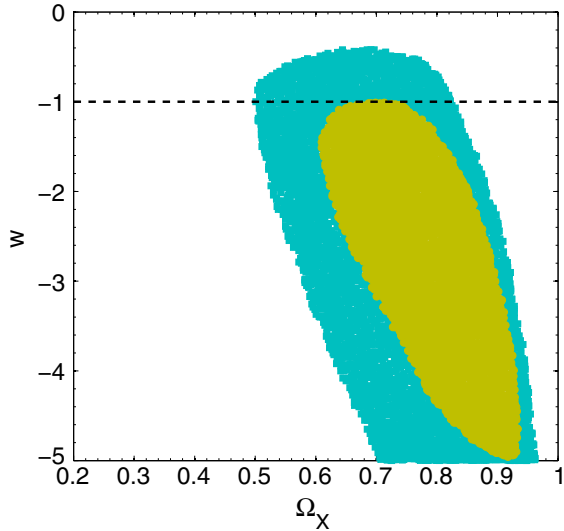


**Figure 3.** Likelihood contours for the flat XCDM model at 68.3% and 95.4% CL in the  $\Omega_x - w$  plane obtained by using Sample A with no redshift evolution. The lower limit on  $w$  is probably an artifact of the prior  $w > -5$  and the horizontal dotted line indicates a cosmological constant with  $w = -1$ .

(A color version of this figure is available in the online journal.)

requires a 20% increase in the characteristic velocity dispersion (i.e.,  $U = 0.25$ ; Oguri et al. 2012). This conclusion is consistent with our results in Section 3.

### 3.2. Constraints on Selected Dark Energy Models

Now, we focus on the constraints obtained on selected dark energy models. Here, we only use Sample A, as results obtained with Sample B are coherent at  $1\sigma$  level.

#### 3.2.1. Dark Energy with Constant Equation of State (XCDM)

When allowing for a deviation from the simple  $w = -1$  case, a component with an arbitrary constant value for the EoS could be introduced. The accelerated expansion is obtained when  $w < -1/3$ . In a zero-curvature universe, the Hubble parameter for this generic dark energy component with density  $\Omega_x$  reads

$$H^2 = H_0^2 [\Omega_m (1+z)^3 + \Omega_x (1+z)^{3(1+w)}]. \quad (16)$$

Obviously, when flatness is assumed ( $\Omega_m + \Omega_\Lambda = 1$ ), it is a two-parameter cosmological model,  $\mathbf{p} = \{\Omega_x, w\}$ .

The best-fit values of the parameters are  $\Omega_x = 0.77 \pm 0.17$ ,  $w = -2.3^{+1.3}_{-2.7}$  with no redshift evolution and  $\Omega_x = 0.79 \pm 0.13$ ,  $w = -2.1^{+1.1}_{-2.8}$  with redshift evolution, see Figures 3 and 4 for the confidence limits in the  $\Omega_x - w$  plane. However, we note that the lower limits on the parameter  $w$  are probably an artifact of the prior  $w > -5$ , which may be tested and constrained with a future larger lens sample. Also in this cosmological scenario, the lens redshift data are consistent with no redshift evolution: when marginalizing over  $\Omega_x$ , we find  $P = -1.4 \pm 1.4$  and  $U = 0.20 \pm 0.28$ . The Einstein's cosmological constant ( $w = -1$ ) is still consistent within  $1\sigma$ . Meanwhile, compared to the cosmological constant model, this flat cosmology with constant EoS dark energy gives a lower  $\chi_{\min}^2$ , but due to one extra parameter it has, it is punished by the information criterion:  $\Delta\text{BIC} = 1.72$  with no redshift evolution and  $\Delta\text{BIC} = 1.55$  with redshift evolution. However, we note that comparing with the cosmological constant model, the two-parameter XCDM model performs relatively well under the information criterion test.

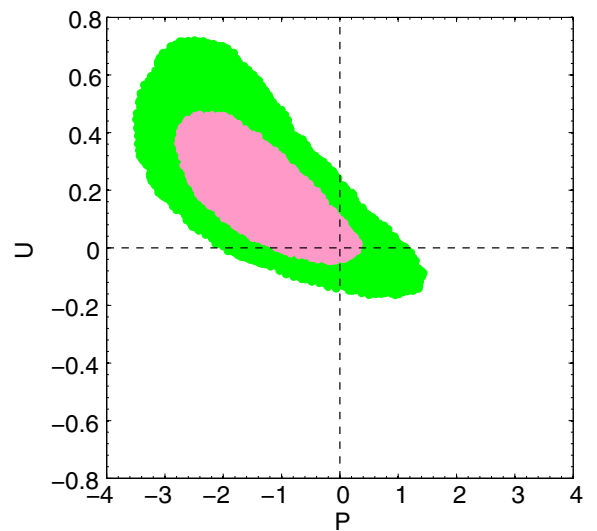
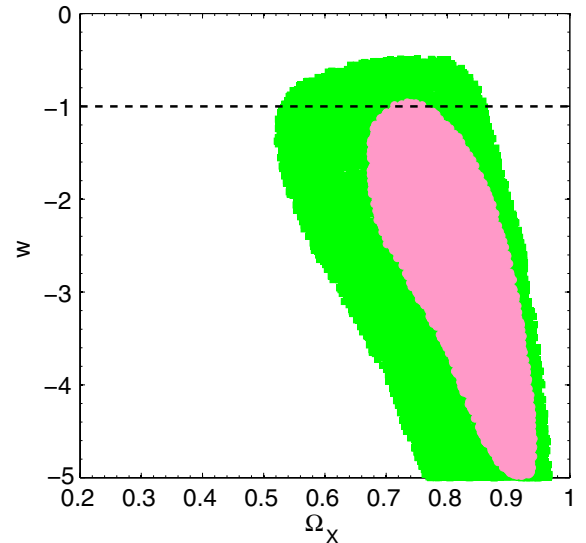


**Figure 4.** As in Figure 1, but for the flat XCDM model obtained by using Sample A with redshift evolution. The lower limit on  $w$  is probably an artifact of the prior  $w > -5$  and the horizontal dotted line indicates a cosmological constant with  $w = -1$ .

(A color version of this figure is available in the online journal.)

#### 3.2.2. Dvali-Gabadadze-Porrati Model (DGP)

The DGP model is generated from the brane world theory in which gravity leaks out into the bulk at large scales and thus leads to the possible accelerated expansion of the universe (Dvali et al. 2000). In this model, the Friedmann equation is modified as follows:

$$3M_{\text{Pl}}^2 \left( H^2 - \frac{H}{r_c} \right) = \rho_m (1+z)^3, \quad (17)$$

where  $M_{\text{Pl}}$  is the Planck mass and  $r_c = (H_0(1 - \Omega_m))^{-1}$  is the crossover scale. For scales below  $r_c$  (where the induced four-dimensional Ricci scalar dominates), the gravitational force is the usual four-dimensional  $1/r^2$  force, whereas for distance scales larger than  $r_c$  the gravitational force follows the five-dimensional  $1/r^3$  behavior. In this model, the Hubble parameter is given by

$$H^2 = H_0^2 \left( \sqrt{\Omega_m (1+z)^3 + \Omega_{r_c}} + \sqrt{\Omega_{r_c}} \right)^2, \quad (18)$$

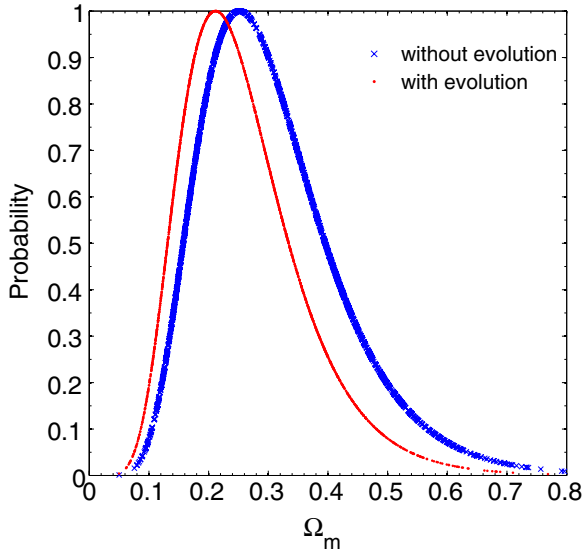


**Figure 5.** Normalized likelihood as a function of  $\Omega_m$  for the DGP model obtained by using Sample A with and without redshift evolution.

(A color version of this figure is available in the online journal.)

where  $\Omega_{rc} = 1/(4r_c^2 H_0^2)$  is a constant. The flat DGP model only contains one free model parameter,  $\mathbf{p} = \{\Omega_m\}$ .

For the DGP model, the best-fit parameters are  $\Omega_m = 0.25^{+0.11}_{-0.09}$  with no redshift evolution and  $\Omega_m = 0.22^{+0.10}_{-0.09}$  with redshift evolution (see Figure 5). We find that the DGP model, as a single-parameter model, is somehow worse than the  $\Lambda$ CDM model, under the present observational test. While its  $\chi^2_{\min}$  is larger than that of the  $\Lambda$ CDM model by about 1.2, it yields  $\Delta\text{BIC} = 1.20$  with no redshift evolution and  $\Delta\text{BIC} = 1.19$  with redshift evolution.

### 3.2.3. Ricci Dark Energy (RDE) Model

There exists a possibility that the average radius of the Ricci scalar curvature  $|\mathcal{R}|^{-1/2}$  might provide an infrared cutoff length scale (Gao et al. 2009). In a flat universe, the Ricci scalar is  $\mathcal{R} = -6(\dot{H} + 2H^2)$  (Gao et al. 2009; Li et al. 2010), and therefore the energy density of the RDE model reads

$$\rho_{de} = 3\beta^2(\dot{H} + 2H^2), \quad (19)$$

where  $\beta$  is a positive constant to be determined. The Hubble parameter can be derived as

$$H^2 = H_0^2 \left[ \frac{2\Omega_m}{2-\beta}(1+z)^3 + \left(1 - \frac{2\Omega_m}{2-\beta}\right)(1+z)^{(4-\frac{2}{\beta})} \right]. \quad (20)$$

This is a two-parameter model with  $\mathbf{p} = \{\Omega_m, \beta\}$ .

For the RDE model, the best-fit values of the parameters are  $\Omega_m = 0.22^{+0.10}_{-0.11}$ ,  $\beta = 0.29 \pm 0.19$  with no redshift evolution; and  $\Omega_m = 0.18^{+0.11}_{-0.12}$ ,  $\beta = 0.28 \pm 0.18$  with redshift evolution. We plot the likelihood contours for the RDE model in the  $\Omega_m - \beta$  plane in Figure 6. Out of all the cosmological models considered in this paper, the RDE model performs the worst, with the largest information criterion result:  $\Delta\text{BIC} = 1.78$  with no redshift evolution, and  $\Delta\text{BIC} = 1.62$  with redshift evolution.

## 4. BIASES AND POSSIBLE SYSTEMATIC EFFECTS

Thus far, we have considered only statistical errors. Indeed, cosmological tests based on strong lensing have been somehow

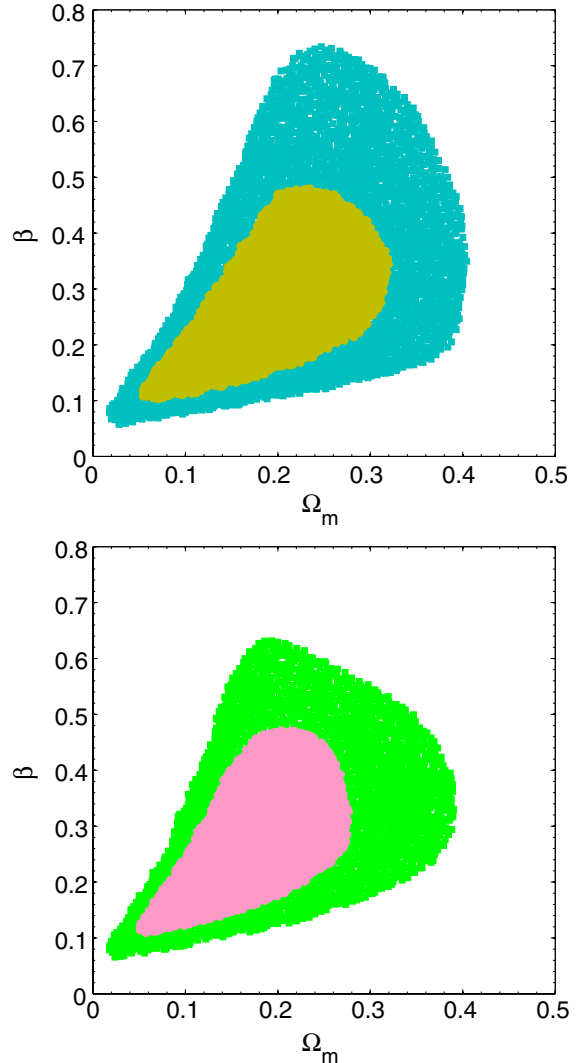


**Figure 6.** Likelihood contours for the RDE model at 68.3% and 95.4% CL obtained by using Sample A with no redshift evolution (upper) and with redshift evolution (lower).

(A color version of this figure is available in the online journal.)

controversial since Kochanek (1996a), in particular for the possible biases associated with sample selection (Capelo & Natarajan 2007). In this section, we discuss several possible sources of systematic errors, including sample incompleteness, unknown survey selection function, uncertainties in the lensing galaxy properties, and lens modeling, in order to verify their effect on the cosmological constraints.

First of all, one general concern is given by the fact that strong gravitational lenses are a biased sample of galaxies. Most of the previous works found no evidence for a biased sample of the lensing population with respect to massive early-type galaxies (see, e.g., Treu et al. 2006). On the other hand, Faure et al. (2011) found possible evidence for the stellar mass of lensing early-type galaxies to evolve significantly with redshift. However, it is still not clear whether this supports a stronger lensing bias toward massive objects at high redshift or if it is a consequence of the possible higher proportion of massive and high stellar density galaxies at high redshift. This could be addressed in dedicated numerical simulations (van de Ven et al. 2009; Mandelbaum et al. 2009), as the available lens samples cannot allow yet to discriminate between the two alternatives.

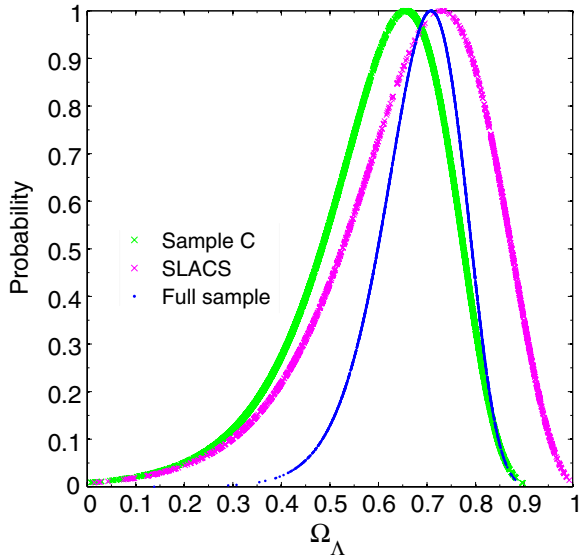


**Figure 7.** Normalized likelihood plot as a function of  $\Omega_\Lambda$  for the flat  $\Lambda$ CDM model, for the three biased samples described in the text.

(A color version of this figure is available in the online journal.)

We now estimate the systematic errors due to statistical sample incompleteness. As both our Samples (A, B) have been put together from different surveys, differences in the observing strategies (and selection functions) may cause systematic errors that are hard to estimate. In order to evaluate the effects due to a selection bias, we have rederived the best estimate on  $\Omega_\Lambda$  (with a no-evolving lens population) by using the whole catalog of  $n = 122$  lenses and two additional, smaller samples (see Table 2): the first one includes only galaxies from the SLACS, and the second one the gravitational lenses with separations no larger than  $2''$ , including 59 and 51 systems, respectively. All of these three samples clearly suffer from strong selection effects or are very inhomogeneous and are therefore not suitable for deriving constraints by means of the redshift distribution test. However, they can shed light on the amplitude of the possible systematic errors due to sample inhomogeneity, incompleteness, and selection bias toward non-representative systems. For instance, it is well known that the SLACS catalog is characterized by a selection function favoring moderately massive ellipticals (e.g., Arneson et al. 2012), also the somehow extreme case of Sample C is not complete (below  $\Delta\theta = 2''$ ) as the probability to detect a lensing galaxy is related to the image separation as very small-separation lenses easily escape detection (both in present-day imaging and spectroscopic surveys). Therefore, we expect that the estimates of  $\Omega_\Lambda$  obtained from these samples allow us to establish an upper limit on the systematic errors due to a not well-defined lens sample.

Results are shown in Figure 7. When using the apparently incomplete sample of small-separation lenses (Sample C), we find  $\Omega_\Lambda = 0.65^{+0.11}_{-0.15}$ . This rather smaller value can be related to the fact that lower-mass lenses, producing small-separation images, will tend to be located at redshifts lower than expected in a large- $\Omega_\Lambda$  model. Hence, this determines a slightly lower value for the cosmological constant.

When adopting the whole SLACS sample, we find  $\Omega_\Lambda = 0.73^{+0.14}_{-0.18}$ . Finally, by considering the whole, inhomogeneous list of 122 lenses, we obtain  $\Omega_\Lambda = 0.71^{+0.07}_{-0.08}$ . When we compare these values with the best estimate obtained from Sample A,

we note that systematic errors do not exceed  $\sim 0.1$  on the cosmological constant.

We have assumed all the lenses to be isolated systems, with negligible line-of-sight contamination. It is well known that the observed image separation may be affected by proximate galaxies and nearby groups of galaxies outside the critical curves of single-lens systems. Indeed, current studies find that proximate galaxies (Cohn & Kochanek 2004) and environmental groups (Keeton & Zabludoff 2004) can have various effects on the primary lens galaxies. However, the most significant effects of the lens-galaxy environments appear to be biasing galaxy ellipticities and image multiplicities. Nevertheless, most of the lenses in Sample B come from the SLACS survey where the role of environment has been assessed in Treu et al. (2009). Namely, it was found that for SLACS lenses, the typical contribution from external mass distribution is no more than a few percent. Therefore, the environmental effects on observed image separations appear to be relatively small (certainly smaller than statistical errors arising from the current sample size of lenses).

In addition to the main lens galaxy, the contribution from line-of-sight density fluctuations to the lens potential should also be taken into consideration. Based on the final lens sample from SQLS, Oguri et al. (2012) have investigated the line-of-sight effect in the form of a constant convergence and shear, and found that its effect on the total lensing probability is rather small compared with the contribution of other systematic errors to the systematic error on  $\Omega_\Lambda$  for the flat models with a cosmological constant (see Table 2 in Oguri et al. 2012). Meanwhile, it is noted that the effect also depends strongly on the image separation, which can have a large impact on lensing probabilities at larger image separations (Oguri et al. 2005; Faure et al. 2009).

Evolution of the VDF and model uncertainties can introduce additional systematic errors. Here, we estimate these systematic errors on the constraint results of the flat  $\Lambda$ CDM with the full sample ( $n = 122$  lenses), in a similar way as done in Oguri et al. (2012). The analysis in Section 3 suggests that unconstrained redshift evolution of the velocity function is one of the most significant sources of systematic error. An additional source of uncertainty is the relation between velocity dispersions and image separations. This uncertainty is not only related to the difference between the velocity dispersion  $\sigma_{\text{SIS}}$  of the mass distribution and the observed stellar velocity dispersion  $\sigma_0$  (White & Davis 1996), but also many complexities such as the velocity dispersion normalization factor for non-spherical galaxies (Oguri et al. 2012) and the detailed luminosity profiles of galaxies.

Hence, we introduce the parameter  $f_E$  that relates the velocity dispersion  $\sigma_{\text{SIS}}$  and the stellar velocity dispersion  $\sigma_0$  as

$$\sigma_{\text{SIS}} = f_E \sigma_0, \quad (21)$$

and the Einstein radius given by Equation (10) is modified to be (Kochanek 1992; Ofek et al. 2003)

$$\Delta\theta_* = 8\pi \left(\frac{\sigma_*}{c}\right)^2 \frac{D_{\text{ls}}}{D_s} f_E^2. \quad (22)$$

The parameter  $f_E$  parameterizes the relation such that  $f_E = 1$  if the velocity dispersion exactly matches the one used for our SIS model. To be more specific, we have kept  $f_E$  as a free parameter, since it mimics the effects of: (1) systematic errors in the rms difference between  $\sigma_0$  (observed stellar velocity dispersion) and

**Table 3**  
Summary of the Priors and Standard Systematic Allowances  
Included in the Analysis

Parameter	Allowance
EoS of DE ( $w$ )	$-5 < w < 0$
DE density in $\Lambda$ CDM ( $\Omega_x$ )	$0 < \Omega_x < 1$
DE density in $\Lambda$ CDM ( $\Omega_\Lambda$ )	$0 < \Omega_\Lambda < 1$
Matter density ( $\Omega_m$ )	$0 < \Omega_m < 1$
Evolution of $n_*$ ( $P$ )	$-10 < P < 10$
Evolution of $\sigma_*$ ( $U$ )	$-1 < U < 1$
Normalization factor ( $f_E$ )	$(0.5)^{1/2} < f_E < (2.0)^{1/2}$
Faint-end slope ( $\alpha$ )	$\alpha = 2.32 \pm 0.10$
High-velocity cutoff ( $\beta$ )	$\beta = 2.67 \pm 0.07$

$\sigma_{\text{SIS}}$  (SIS model velocity dispersion); (2) softened isothermal sphere potentials which tend to decrease the typical image separations (Narayan & Bartelmann 1996); (3) the influence of line-of-sight mass contamination, with the significant effect of the large-scale structure on strong lensing (Keeton et al. 1997); and (4) the effect of secondary lenses (satellites, nearby galaxies, groups, etc.) on observed image separation. All of the above factors can possibly affect the images separation by up to  $\pm 20\%$  (Ofek et al. 2003). More recently, by combining stellar kinematics (central velocity dispersion measurements) with lensing geometry (Einstein radius determination from position of images), Cao et al. (2012) have tested a combined gravitational lens data set including 70 data points from SLACS and LSD, and obtained consistent results.

We consider the flat models with a cosmological constant, and obtain simultaneous constraints on  $\Omega_\Lambda$  and  $f_E$  with the full sample ( $n = 122$  lenses). The constraint result, shown in Figure 8, indicates that constraints on  $f_E$  from the data in our analysis are degenerate with  $\Omega_\Lambda$ . The marginalized constraints on each parameter are  $f_E = 1.08 \pm 0.14$  and  $\Omega_\Lambda = 0.65^{+0.35}_{-0.45}$ . Thus, the cosmological constraints become much weaker, although models with a significant cosmological constant are still preferred. A vanishing cosmological constant is still ruled at  $1\sigma$ .

The slightly larger value of  $f_E$  demonstrates that lens statistics with  $f_E = 1$  favor slightly larger  $\Omega_\Lambda$  and that the observed mean image separation appears to be slightly higher than the models predict (Capelo & Natarajan 2007). However, models with  $f_E = 1$  are consistent with the data to better than  $2\sigma$ . To be more specific, in order to take into account the measurement uncertainty and the approximations we are doing (no lens ellipticity accounted and no external shear), we estimate a fiducial error of  $\sim 5\%$  on the values of image separations (Grillo et al. 2008), which is equivalent to a  $\sim 5\%$  uncertainty on the parameter  $f_E^2$ .

The velocity distribution function given by Equation (6) is another important source of systematic error on the final results. While adopting the best-fit values of the VDF measurement in the SDSS Data Release 5 by Choi et al. (2007) as our fiducial model, we investigate how the cosmological results are altered by introducing the uncertainties on  $\alpha$  and  $\beta$  as listed in Table 3. With the results of measurements on the VDF, we vary the parameter of interest while fixing the other parameters at their best-fit values. For example, based on the  $n = 122$  sample, we vary the faint-end slope  $\alpha$  by  $\pm 0.10$  and find that this effect is quite negligible when compared to the present accuracy of the test (Mitchell et al. 2005).

The complete set of standard priors and allowances included in the analysis of the above systematics is summarized in Table 3.

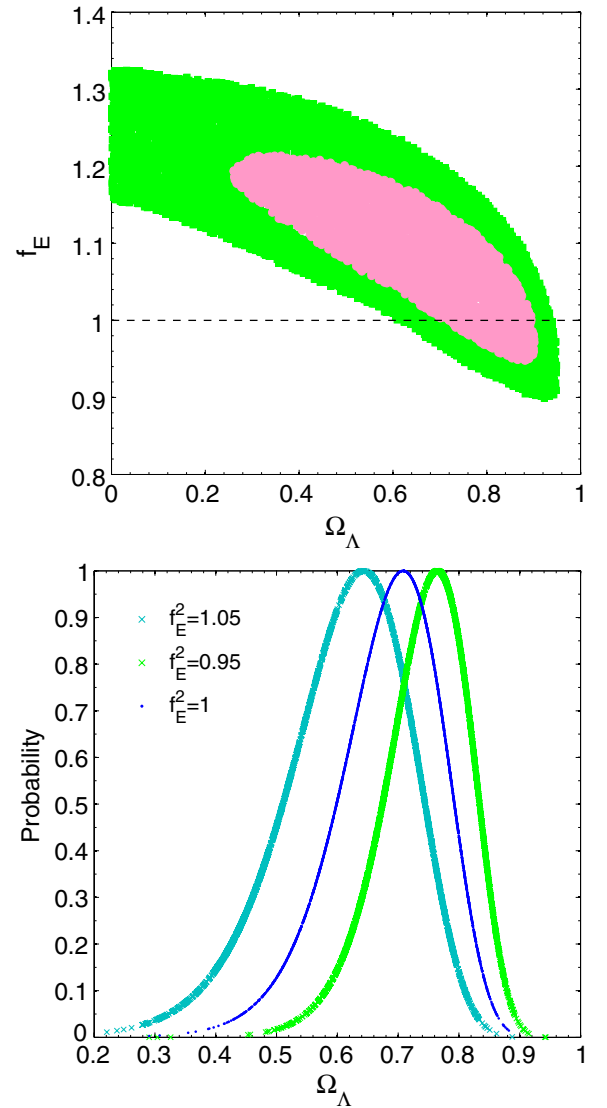


**Figure 8.** Upper panel: constraint results on the cosmological constant  $\Omega_\Lambda$  and the parameter  $f_E$  in Equation (22) that parameterizes the relation between velocity dispersions and image separations, for the flat  $\Lambda$ CDM model with the full sample ( $n = 122$  lenses). The horizontal dashed line indicates the fiducial value  $f_E = 1$  assumed in the paper. Lower panel: constraints on  $\Omega_\Lambda$  with different values of  $f_E$  considering a fiducial error of  $\sim 5\%$  on the values of image separations.

(A color version of this figure is available in the online journal.)

By comparing the contribution of each of these systematic errors to the systematic error on  $\Omega_\Lambda$  for the flat models with a cosmological constant with the full sample, as shown in Figures 8 and 9 and Table 4, we find that the largest sources of systemic error are the dynamical normalization  $f_E$  and the high-velocity cutoff  $\beta$ , followed by the faint-end slope  $\alpha$  of the velocity dispersion function. The finding is consistent with the earlier results in Oguri et al. (2012). This result remains consistent with the current standard cosmological model ( $\Omega_x \sim 0.7$ ,  $\Omega_m \sim 0.3$ , and  $w \sim -1$ ). Indeed, current samples of lenses do not allow us to discriminate between an  $\Omega_\Lambda$  and a dynamical dark energy component.

## 5. CONCLUSION AND DISCUSSION

Since the discovery of the accelerating expansion of the universe, in addition to the standard  $\Lambda$ CDM cosmological

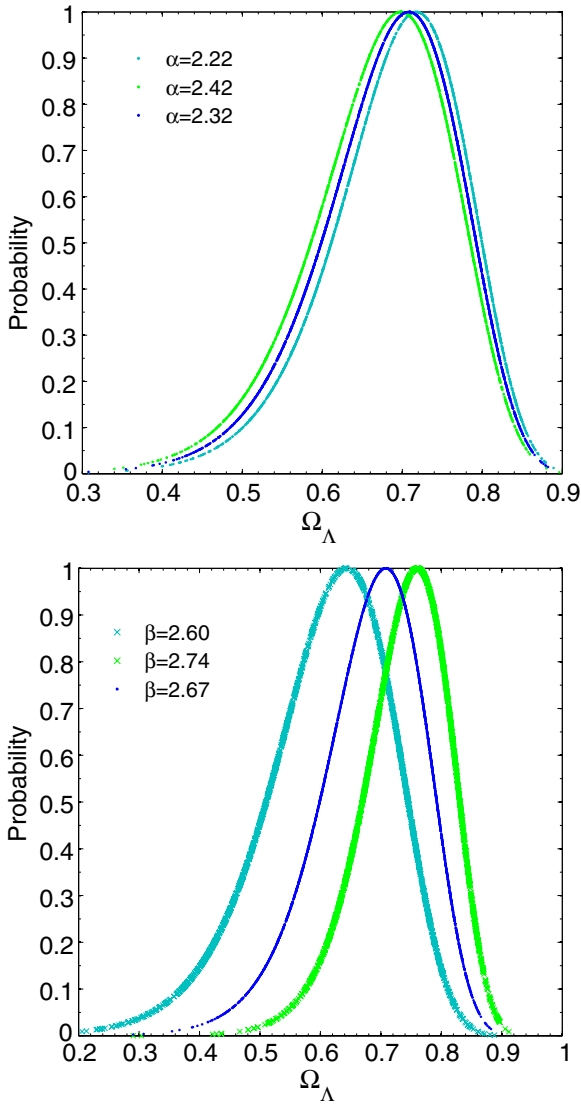


**Figure 9.** Normalized likelihood plot for the flat  $\Lambda$ CDM model with the full sample ( $n = 122$  lenses), by introducing the uncertainties on the VDF parameters: the faint-end slope  $\alpha$  and the high-velocity cutoff  $\beta$ , as listed in Table 3.

(A color version of this figure is available in the online journal.)

model, a large number of theoretical scenarios have been proposed for the acceleration mechanism. Examples include the quintessence (Ratra & Peebles 1988; Caldwell et al. 1998), phantom (Caldwell 2002), quintom (Feng et al. 2005, 2006; Guo et al. 2005), and the Chaplygin gas (Kamenshchik et al. 2001; Bento et al. 2002; Alam et al. 2003; Zhu 2004; Zhang & Zhu 2006). All these acceleration mechanisms should be tested with various astronomical observations, such as SNe Ia, *WMAP* (Komatsu et al. 2009), and BAO (Percival et al. 2007). However, it is still important to use many different observational probes to set bounds on cosmological parameters. In this work, we have followed this direction and used the redshift distribution of two well-defined samples of lensing, elliptical galaxies drawn from a large catalog of 122 gravitational lenses from a variety of surveys (see Table 1). To assess various competing dark energy models and make a comparison, the BIC is also applied in this analysis.

Considering the two cases with and without the redshift evolution of the velocity function of galaxies, we have analyzed

**Table 4**  
Constraint Results Obtained by the Full Sample ( $n = 122$  lenses) for the Flat  $\Lambda$ CDM Model with Different Systematic Errors

Systematics	$\Omega_\Lambda$
$f_E^2 = 1.00$ ; $\alpha = 2.32$ ; $\beta = 2.67$	$\Omega_\Lambda = 0.71^{+0.07}_{-0.08}$
$f_E^2 = 0.95$ ; $\alpha = 2.32$ ; $\beta = 2.67$	$\Omega_\Lambda = 0.76^{+0.06}_{-0.07}$
$f_E^2 = 1.05$ ; $\alpha = 2.32$ ; $\beta = 2.67$	$\Omega_\Lambda = 0.65^{+0.08}_{-0.12}$
$f_E^2 = 1.00$ ; $\alpha = 2.22$ ; $\beta = 2.67$	$\Omega_\Lambda = 0.72^{+0.08}_{-0.09}$
$f_E^2 = 1.00$ ; $\alpha = 2.42$ ; $\beta = 2.67$	$\Omega_\Lambda = 0.70^{+0.08}_{-0.10}$
$f_E^2 = 1.00$ ; $\alpha = 2.32$ ; $\beta = 2.60$	$\Omega_\Lambda = 0.64^{+0.08}_{-0.10}$
$f_E^2 = 1.00$ ; $\alpha = 2.32$ ; $\beta = 2.74$	$\Omega_\Lambda = 0.76 \pm 0.07$

**Table 5**  
Summary of the Constraint Results and Information Criterion with Sample A

Model	Constraint Result	$\Delta$ BIC
$\Lambda$ CDM ( $P = U = 0$ )	$\Omega_\Lambda = 0.70 \pm 0.09$	0
( $P \neq U \neq 0$ )	$\Omega_\Lambda = 0.73 \pm 0.09$	0
XCDM ( $P = U = 0$ )	$\Omega_x = 0.77 \pm 0.17$ ; $w = -2.3^{+1.3}_{-2.7}$	1.72
( $P \neq 0 \neq 0$ )	$\Omega_x = 0.79 \pm 0.13$ ; $w = -2.1^{+1.1}_{-2.8}$	1.55
DGP ( $P = U = 0$ )	$\Omega_m = 0.25^{+0.11}_{-0.09}$	1.20
( $P \neq U \neq 0$ )	$\Omega_m = 0.22^{+0.10}_{-0.09}$	1.19
RDE ( $P = U = 0$ )	$\Omega_m = 0.22^{+0.10}_{-0.11}$ ; $\beta = 0.29 \pm 0.19$	1.78
( $P \neq U \neq 0$ )	$\Omega_m = 0.18^{+0.11}_{-0.12}$ ; $\beta = 0.28 \pm 0.18$	1.62

**Note.** The  $\Delta$ BIC values for all other models are measured with respect to the cosmological constant model.

four dark energy models (the  $\Lambda$ CDM, the XCDM with constant  $w$ , the DGP, and the RDE models) under a flat universe assumption. For each model, we have calculated the best-fit values of its parameters and found its  $\Delta$ BIC value. Results are plotted in Figures 1–6.

The fit and information criteria results have been summarized in Table 5. The cosmological constant model has the lowest value of BIC and the value of  $\Delta$ BIC is measured with respect to this model. It is shown that for the zero-curvature  $\Lambda$ CDM model, the likelihood is maximized, for  $\Omega_\Lambda = 0.70 \pm 0.09$  with no redshift evolution and  $\Omega_\Lambda = 0.73 \pm 0.09$  with redshift evolution, when using the Sample A (see Section 2). Consistent results (within  $1\sigma$ ) are derived when the alternative Sample B is considered.

We have also derived simultaneous constraints on the redshift evolution of the parameters  $n_*$  and  $\sigma_*$  of the velocity function. The constraints in the  $P - U$  plane also indicate that the data are consistent with the no-redshift-evolution case ( $P = 0$ ;  $U = 0$ ) at  $1\sigma$ , with  $P = -1.2 \pm 1.4$  and  $U = 0.22^{+0.26}_{-0.27}$ . Both in the no-evolution and galaxy evolution scenario, we rule out with high confidence a vanishing cosmological constant, with both of the lens samples (at confidence larger than  $\sim 4\sigma$ ), as recently found by Oguri et al. (2012) by adopting a smaller and independent lens sample. Therefore, the redshift test adds an independent evidence to the accelerating expansion.

The obtained likelihood distributions shown in Figure 1 are also in agreement with the results from analyzing data of *WMAP* 5-year results with the BAO and SNe Union data, and the large-scale structures in the SDSS luminous red galaxies (Spergel et al. 2003; Tegmark et al. 2004; Eisenstein et al. 2005), which implies that gravitational lensing statistics provide an independent and complementary support on the  $\Lambda$ CDM model.

We give a graphical representation of the BIC test in Figure 10. Following the  $\Lambda$ CDM model, The DGP model is the only one-parameter model that gives a worse fit but also

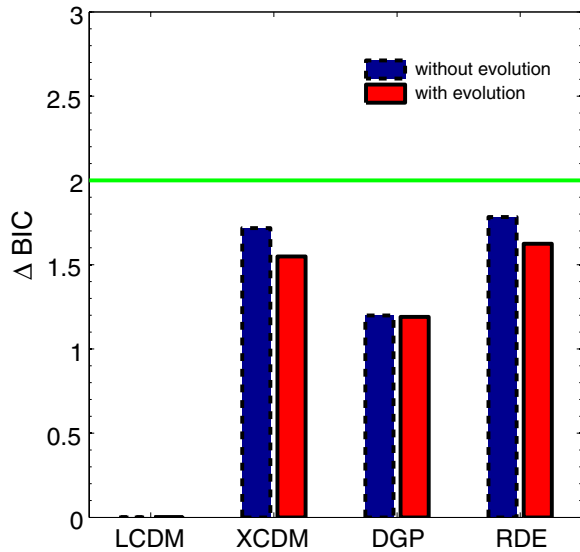


**Figure 10.** Graphical representation of the results in Table 5: the values of  $\Delta\text{BIC}$  for each model, relative to the LCDM ( $\Lambda\text{CDM}$ ). The order of models from left to right is the same as that in Table 5. The horizontal green line indicates  $\Delta\text{BIC} = 2$ , which is considered positive evidence against the model with the higher BIC.

(A color version of this figure is available in the online journal.)

reduces to the  $\Lambda\text{CDM}$ , as we obtained close values for the matter density. The XCDM model gives a comparably good fit, but has one additional free parameter, that is in accordance with the best-fit  $\Lambda\text{CDM}$  model (within  $1\sigma$  range for the EoS parameter). The other two-parameter model, RDE, provides a worse fit to the data, though the difference in BIC ( $\Delta\text{BIC}$ ) indicates no clear evidence against it. Therefore, while still not firmly ruling out competing world models, the redshift distribution test clearly favors the cosmological constant model, a conclusion in accordance with previous works (Davis et al. 2007).

In order to assess the reliability of our results and the related systematic errors, we have introduced three additional lens samples, characterized by different degrees of inhomogeneity and incompleteness, and rederived an estimate for the cosmological constant assuming a not-evolving lens population. Two lens samples (the whole heterogeneous catalog of 122 systems and the SLACS sample) give results fully consistent with those discussed above, confirming for us that systematic errors due to sample selection are not larger than statistical uncertainties.

Our model involves several uncertainties and assumptions that introduce additional systematic errors in our cosmological analysis (see Table 3). By comparing the contribution of each of these systematic errors to the systematic error on the flat  $\Lambda\text{CDM}$  model (see Figures 8 and 9 and Table 4), we find that the largest sources of systematic error are the dynamical normalization and the high-velocity cutoff factor, followed by the faint-end slope of the velocity dispersion function, which is consistent with the earlier results in Oguri et al. (2012). Moreover, the comparable systematic errors suggest the importance of careful studies of the systematics for robust cosmological constraints from lens statistics.

Finally, we note that four important effects, neglected here, should be mentioned. Evolution of the source population can also matter to the technique applied in this paper, which might have a small second-order effect on the statistics (Oguri et al. 2012). We have also neglected systematic uncertainties due to the effect of small-scale inhomogeneities on large-scale obser-

vations. Indeed, matter distribution is locally inhomogeneous and affects light propagation and the related cosmological distances (Serenio et al. 2001, 2002). However, the universe being globally homogeneous, the effect on the total lensing statistics is small (Covone et al. 2005). Meanwhile, though the lens redshift test applied in this paper is free from the magnification bias arising from the uncertain source counts, it may also lose the statistical power of absolute lensing probabilities. The last one is that multiple errors or biases in the method could easily be canceled out, which may lead the result to be a statistical fluke (Maoz 2005).

Despite some of its inherent difficulties, the redshift distribution test, with either larger gravitational lensing samples from future wide-field surveys such as Pan-STARRS and Large Synoptic Survey Telescope by taking advantage of time-domain information (Oguri & Marshall 2010) or a joint investigation with other cosmological observations, could be helpful for advancing such applications and provide more stringent constraints on the cosmological parameters.

We acknowledge fruitful discussions with M. Paolillo. We thank the anonymous referee for valuable comments which helped us to improve the paper. G.C. thanks I. Skripnikova for enlightening discussions.

This work was supported by the National Natural Science Foundation of China under the Distinguished Young Scholar Grant 10825313, the Ministry of Science and Technology national basic science Program (Project 973) under grant No. 2012CB821804, the Fundamental Research Funds for the Central Universities and Scientific Research Foundation of Beijing Normal University, and the Excellent Doctoral Dissertation of Beijing Normal University Engagement Fund.

## REFERENCES

- Alam, U., Sahni, V., Saini, T. D., & Starobinsky, A. A. 2003, *MNRAS*, **334**, 1057
- Alcaniz, J. S. 2002, *Phys. Rev. D*, **65**, 123514
- Alcaniz, J. S., Jain, D., & Dev, A. 2003, *Phys. Rev. D*, **67**, 043514
- Amani, A. R. 2011, *Int. J. Theor. Phys.*, **50**, 3078
- Anguita, T., Faure, C., Kneib, J.-P., et al. 2009, *A&A*, **507**, 35
- Arneson, R. A., Brownstein, J. R., & Bolton, A. S. 2012, *ApJ*, **753**, 4
- Bennett, C. L., Halpern, M., Hinshaw, G., et al. 2003, *ApJS*, **148**, 1
- Bento, M. C., Bertolami, O., & Sen, A. A. 2002, *Phys. Rev. D*, **66**, 043507
- Biesiada, M., Piórkowska, A., & Malec, B. 2010, *MNRAS*, **406**, 1055
- Biggs, A. D., Rusin, D., Browne, I. W. A., et al. 2003, *MNRAS*, **338**, 1084
- Blackburne, J. A., Wisotzki, L., & Schechter, P. L. 2008, *AJ*, **135**, 374
- Bolton, A. S., Bures, S., Koopmans, L. E. V. E., et al. 2008, *ApJ*, **682**, 964
- Brown, M. J. I., Dey, A., Jannuzi, B. T., et al. 2007, *ApJ*, **654**, 858
- Burud, I., Courbin, F., Magain, P., et al. 2002a, *A&A*, **383**, 71
- Burud, I., Hjorth, J., Courbin, F., et al. 2002b, *A&A*, **391**, 481
- Caldwell, R. 2002, *Phys. Lett. B*, **545**, 23
- Caldwell, R., Dave, R., & Steinhardt, P. J. 1998, *Phys. Rev. Lett.*, **80**, 1582
- Cao, S., Liang, N., & Zhu, Z.-H. 2011a, *MNRAS*, **416**, 1099
- Cao, S., Pan, Y., Biesiada, M., Godlowski, W., & Zhu, Z.-H. 2012, *J. Cosmol. Astropart. Phys.*, **JCAP03(2012)016**
- Cao, S., & Zhu, Z.-H. 2012, *A&A*, **538**, A43
- Cao, S., Zhu, Z.-H., & Liang, N. 2011b, *A&A*, **529**, A61
- Cao, S., Zhu, Z.-H., & Zhao, R. 2011c, *Phys. Rev. D*, **84**, 023005
- Capelo, P. R., & Natarajan, P. 2007, *New J. Phys.*, **9**, 445
- Chae, K.-H. 2003, *MNRAS*, **346**, 746
- Chae, K.-H. 2007, *ApJ*, **658**, L71
- Chae, K.-H., Biggs, A. D., Blandford, R. D., et al. 2002, *Phys. Rev. Lett.*, **89**, 151301
- Chiba, M., & Yoshii, Y. 1999, *ApJ*, **510**, 42
- Choi, Y.-Y., Park, C., & Vogeley, M. S. 2007, *ApJ*, **658**, 884
- Cohen, J. G., Lawrence, C. R., & Blandford, R. D. 2003, *ApJ*, **583**, 67
- Cohn, J. D., & Kochanek, C. S. 2004, *ApJ*, **608**, 25
- Cooray, A. R., & Huterer, D. 1999, *ApJ*, **513**, L95
- Covone, G., Sereno, M., & de Ritis, R. 2005, *MNRAS*, **357**, 773

- Crampton, D., Schade, D., Hammer, F., et al. 2002, *ApJ*, 570, 86
- Davis, T. M., Mörtzell, E., Sollerman, J., et al. 2007, *ApJ*, 666, 716
- Durrer, R., & Maartens, R. 2010, in *Dark Energy: Observational & Theoretical Approaches*, ed. P. Ruiz-Lapuente (Cambridge: Cambridge Univ. Press), 48
- Dvali, G., Gabadadze, G., & Porrati, M. 2000, *Phys. Lett. B*, 485, 208
- Eigenbrod, A., Courbin, F., Meylan, G., Vuissoz, C., & Magain, P. 2006, *A&A*, 451, 759
- Eisenhardt, P. R., Armus, L., Hogg, D. W., et al. 1996, *ApJ*, 461, 72
- Eisenstein, D. J., Zehavi, I., Hogg, D. W., et al. 2005, *ApJ*, 633, 560
- Faber, S. M., Willmer, C. N. A., Wolf, C., et al. 2007, *ApJ*, 665, 265
- Falco, E. E., Lehár, J., & Shapiro, I. I. 1997, *AJ*, 113, 540
- Fang, W., Wang, S., Hu, W., et al. 2008, *Phys. Rev. D*, 78, 103509
- Fassnacht, C. D., Blandford, R. D., Cohen, J. G., et al. 1999, *AJ*, 117, 658
- Fassnacht, C. D., & Cohen, J. G. 1998, *AJ*, 115, 377
- Fassnacht, C. D., Womble, D. S., Neugebauer, G., et al. 1996, *ApJ*, 460, L103
- Faure, C., Anguita, T., Alloin, D., et al. 2011, *A&A*, 529, A72
- Faure, C., Kneib, J.-P., Covone, G., et al. 2008, *ApJS*, 176, 19
- Faure, C., Kneib, J.-P., Hilbert, S., et al. 2009, *ApJ*, 695, 1233
- Feng, B., Li, M., Piao, Y., & Zhang, X. 2006, *Phys. Lett. B*, 634, 101
- Feng, B., Wang, X., & Zhang, X. 2005, *Phys. Lett. B*, 607, 35
- Feng, C. J., & Li, X. Z. 2009, *Phys. Lett. B*, 680, 184
- Fukugita, M., Futamase, T., & Kasai, M. 1990, *MNRAS*, 246, 24P
- Gao, C., Wu, F., Chen, X., Shen, Y.-G., et al. 2009, *Phys. Rev. D*, 79, 043511
- Gaztañaga, E., Cabré, A., & Hui, L. 2009, *MNRAS*, 399, 1663
- Gregg, M. D., Lacy, M., White, R. L., et al. 2002, *ApJ*, 564, 133
- Gregg, M. D., Wisotzki, L., Becker, R. H., et al. 2000, *AJ*, 119, 2535
- Grillo, C., Lombardi, M., & Bertin, G. 2008, *A&A*, 477, 397
- Guo, Z. K., Piao, Y., Zhang, X., & Zhang, Y. 2005, *Phys. Lett. B*, 608, 177
- Hagen, H.-J., & Reimers, D. 2000, *A&A*, 357, L29
- Hall, P. B., Richards, G. T., York, D. G., et al. 2002, *ApJ*, 575, L51
- Helbig, P., & Kayser, R. 1996, *A&A*, 308, 359
- Hewett, P. C., Irwin, M. J., Foltz, C. B., et al. 1994, *AJ*, 108, 1534
- Hinshaw, G., Weiland, J. L., Hill, R. S., et al. 2008, *ApJS*, 180, 225
- Huchra, J., Gorenstein, M., Kent, S., et al. 1985, *AJ*, 90, 691
- Im, M., Simard, L., Faber, S. M., et al. 2002, *ApJ*, 571, 136
- Inada, N., Burles, S., Gregg, M. D., et al. 2005, *AJ*, 130, 1967
- Inada, N., Oguri, M., Becker, R. H., et al. 2008, *AJ*, 135, 496
- Johnston, D. E., Richards, G. T., Frieman, J. A., et al. 2003, *AJ*, 126, 2281
- Kamenshchik, A., Moschella, U., & Pasquier, V. 2001, *Phys. Lett. B*, 511, 265
- Kang, X., Jing, Y. P., Mo, H. J., & Börner, G. 2005, *ApJ*, 631, 21
- Keeton, C. R., Kochanek, C. S., & Seljak, U. 1997, *ApJ*, 482, 604
- Keeton, C. R., & Zabludoff, A. I. 2004, *ApJ*, 612, 660
- Kneib, J., Cohen, J. G., & Hjorth, J. 2000, *ApJ*, 544, L35
- Kochanek, C. S. 1992, *ApJ*, 384, 1
- Kochanek, C. S. 1996a, *ApJ*, 466, 638
- Kochanek, C. S. 1996b, *ApJ*, 473, 595
- Kochanek, C. S., Falco, E. E., Impey, C. D., et al. 2000, *ApJ*, 543, 131
- Komatsu, E., Dunkley, J., Nolte, M. R., et al. (WMAP Collaboration) 2009, *ApJS*, 180, 330
- Koopmans, L. V. E., & Treu, T. 2002, *ApJ*, 568, L5
- Koopmans, L. V. E., & Treu, T. 2003, *ApJ*, 583, 606
- Lacy, M., Gregg, M., Becker, R. H., et al. 2002, *AJ*, 123, 2925
- Lagattuta, D. J., Fassnacht, C. D., Auger, M. W., et al. 2010, *ApJ*, 716, 1579
- Langston, G. I., Schneider, D. P., Conner, S., et al. 1989, *AJ*, 97, 1283
- Lehár, J., Falco, E. E., Kochanek, C. S., et al. 2000, *ApJ*, 536, 584
- Lehár, J., Langston, G. I., Silber, A., Lawrence, C. R., & Burke, B. F. 1993, *AJ*, 105, 847
- Lewis, A., & Bridle, S. 2002, *Phys. Rev. D*, 66, 103511
- Li, M., Li, X., & Zhang, X. 2010, *Sci. China Phys. Mech. Astron.*, 53, 1631
- Lidman, C., Courbin, F., Kneib, J.-P., et al. 2000, *A&A*, 364, L62
- Lubin, L. M., Fassnacht, C. D., Readhead, A. C. S., Blandford, R. D., & Kundić, T. 2000, *AJ*, 119, 451
- Maartens, R., & Koyama, K. 2010, *Living Rev. Relat.*, 13, 5
- Mandelbaum, R., van de Ven, G., & Keeton, C. R. 2009, *MNRAS*, 398, 2
- Maoz, D. 2005, in *IAU Symp. 225, Impact of Gravitational Lensing on Cosmology Proceedings*, ed. Y. Mellier & G. Meylan (Cambridge: Cambridge Univ. Press), 413
- Maoz, D., & Rix, H.-W. 1993, *ApJ*, 416, 425
- Mitchell, J. L., Keeton, C. R., Frieman, J. A., & Sheth, R. K. 2005, *ApJ*, 622, 81
- Morgan, N. D., Becker, R. H., Gregg, M. D., Schechter, P. L., & White, R. L. 2001, *AJ*, 121, 611
- Morgan, N. D., Caldwell, J. A. R., Schechter, P. L., et al. 2004, *AJ*, 127, 2617
- Moustakas, L. A., Marshall, P., Newman, J. A., et al. 2007, *ApJ*, 660, L31
- Muñoz, J. A., Falco, E. E., Kochanek, C. S., et al. 2001, *ApJ*, 546, 769
- Myers, S. T., Rusin, D., Fassnacht, C. D., et al. 1999, *AJ*, 117, 2565
- Narayan, R., & Bartelmann, M. 1996, in *Lectures on Gravitational Lensing, Formation of Structure in the Universe*, ed. A. Dekel & J. P. Ostriker (Cambridge: Cambridge University Press), (arXiv:astro-ph/9606001)
- Nemiroff, R. J. 1989, *ApJ*, 341, 579
- Newton, E. R., Marshall, P. J., Treu, T., et al. 2011, *ApJ*, 734, 104
- O'Dea, C. P., Baum, S. A., Stanghellini, C., et al. 1992, *AJ*, 104, 1320
- Ofek, E. O., Maoz, D., Rix, H.-W., Kochanek, C. S., & Falco, E. E. 2006, *ApJ*, 641, 70
- Ofek, E. O., Rix, H.-W., & Maoz, D. 2003, *MNRAS*, 343, 639
- Oguri, M., Inada, N., Strauss, M. A., et al. 2012, *AJ*, 143, 120
- Oguri, M., Keeton, C. R., & Dalal, N. 2005, *MNRAS*, 364, 1451
- Oguri, M., & Marshall, P. J. 2010, *MNRAS*, 405, 2579
- Percival, W. J., Cole, S., Eisenstein, D. J., et al. 2007, *MNRAS*, 381, 1053
- Perlmutter, S., Aldering, G., Goldhaber, G., et al. 1999, *ApJ*, 517, 565
- Pires, N., Zhu, Z.-H., & Alcaniz, J. S. 2006, *Phys. Rev. D*, 73, 123530
- Ratnatunga, K. U., Griffiths, R. E., & Ostrander, E. J. 1999, *AJ*, 117, 2010
- Ratra, B., & Peebles, P. E. J. 1988, *Phys. Rev. D*, 37, 3406
- Riess, A. G., Filippenko, A. V., Challis, P., et al. 1998, *AJ*, 116, 1009
- Ruff, A. J., Gavazzi, R., Marshall, P. J., et al. 2011, *ApJ*, 727, 96
- Schechter, P. 2005, in *IAU Symp. 225, The Impact of Gravitational Lensing on Cosmology*, ed. Y. Mellier & G. Meylan (Cambridge, UK: Cambridge University Press), 281
- Schechter, P. L., Gregg, M. D., Becker, R. H., Helfand, D. J., & White, R. L. 1998, *AJ*, 115, 1371
- Schwarz, G. 1978, *Ann. Stat.*, 6, 461
- Sereno, M. 2002, *A&A*, 393, 757
- Sereno, M. 2005, *MNRAS*, 356, 977
- Sereno, M., Covone, G., Piedipalumbo, E., & de Ritis, R. 2001, *MNRAS*, 327, 517
- Sereno, M., & Longo, G. 2004, *MNRAS*, 354, 1255
- Sereno, M., Piedipalumbo, E., & Sazhin, M. V. 2002, *MNRAS*, 335, 1061
- Sheth, R. K., Bernardi, M., Schechter, P. L., et al. 2003, *ApJ*, 594, 225
- Siemiginowska, A., Bechtold, J., Aldcroft, T. L., McLeod, K. K., & Keeton, C. R. 1998, *ApJ*, 503, 118
- Sluse, D., Surdej, J., Claeskens, J.-F., et al. 2003, *A&A*, 406, L43
- Spergel, D. N., Verde, L., Peiris, H. V., et al. 2003, *ApJS*, 148, 175
- Stern, D., Jimenez, R., Verde, L., Kamionkowski, M., & Stanford, S. A. 2010, *J. Cosmol. Astropart. Phys.*, JCAP02(2010)008
- Surdej, J., Claeskens, J.-F., Remy, M., et al. 1997, *A&A*, 327, L1
- Sykes, C. M., Browne, I. W. A., Jackson, N. J., et al. 1998, *MNRAS*, 301, 310
- Tegmark, M., Strauss, M. A., Blanton, M. R., et al. 2004, *Phys. Rev. D*, 69, 103501
- Tonry, J. L. 1998, *AJ*, 115, 1
- Tonry, J. L., & Kochanek, C. S. 1999, *AJ*, 117, 2034
- Treu, T., Gavazzi, R., Gorecki, A., et al. 2009, *ApJ*, 690, 670
- Treu, T., & Koopmans, L. V. E. 2004, *ApJ*, 611, 739
- Treu, T., Koopmans, L. V. E., Bolton, A. S., Burles, S., & Moustakas, L. A. 2006, *ApJ*, 640, 662
- van de Ven, G., Mandelbaum, R., & Keeton, C. R. 2009, *MNRAS*, 398, 2
- White, R. E., & Davis, D. S. 1996, *BAAS*, 28, 1323
- Wiklund, T., & Combes, F. 1995, *A&A*, 299, 382
- Wiklund, T., & Combes, F. 1996, *Nature*, 379, 139
- Winn, J. N., Hewitt, J. N., Schechter, P. L., et al. 2000, *AJ*, 120, 2868
- Winn, J. N., Lovell, J. E. J., Chen, H.-W., et al. 2002a, *ApJ*, 564, 143
- Winn, J. N., Morgan, N. D., Hewitt, J. N., et al. 2002b, *AJ*, 123, 10
- Wisotzki, L., Schechter, P. L., Bradt, H. V., Heinmüller, J., & Reimers, D. 2002, *A&A*, 395, 17
- Yamamoto, K., & Futamase, T. 2001, *Prog. Theor. Phys.*, 105, 707
- Zhang, H., & Zhu, Z.-H. 2006, *Phys. Rev. D*, 73, 043518
- Zhu, Z.-H. 1998, *A&A*, 338, 777
- Zhu, Z.-H. 2004, *A&A*, 423, 421
- Zhu, Z.-H., & Alcaniz, J. S. 2005, *ApJ*, 620, 7
- Zhu, Z.-H., & Fujimoto, M. K. 2002, *ApJ*, 581, 1
- Zhu, Z.-H., & Sereno, M. 2008, *A&A*, 487, 831